INTERNATIONAL JOURNAL OF CLIMATOLOGY
Int. J. Climatol. **37**: 548–558 (2017)
Published online 5 April 2016 in Wiley Online Library
(wileyonlinelibrary.com) DOI: 10.1002/joc.4713

RMetS
Royal Meteorological Society

Short Communication

Unveiling the multiscale teleconnection between Pacific Decadal Oscillation and global surface temperature using time-dependent intrinsic correlation analysis

Adarsh Sankaran*

Department of Civil Engineering, TKM College of Engineering, Kollam, India

ABSTRACT: Global surface temperature is significantly influenced by different climate forcings operating at specific time scales. This study investigates the association between global surface temperature and the Pacific Decadal Oscillation (PDO) in a multiscaling framework in terms of both time scale of variability and non-stationarity. First, the ensemble empirical mode decomposition (EEMD) is used for multiscale disintegration of the Global Surface Temperature Anomaly (GSTA) and PDO datasets. A close matching of the periodicity of different modes of PDO and GSTA is noticed, and the subsequent cross-correlation analysis of the modes showed that their linear association is the most perceptible at the slowly varying trend component. The correlation between the different modes is further analyzed using a multiscale dynamic correlation method namely, time-dependent intrinsic correlation (TDIC). This study found a strong long-range positive correlation between the time series pairs in decadal and inter-decadal modes exceeding 20-year periodicity. Further it is found that, the multiscale teleconnection between PDO and GSTA is not always of unique character but associated with localized reversals in the nature of correlation in the time domain. The study further observed a similar pattern of correlation for both cold phases of the 20th century (1901–1924 and 1947–1976); whereas the pattern of correlation is different for the warm phases of PDO (1925–1946 and 1977–1995) in different process scales.

KEY WORDS ensemble empirical mode decomposition; multiscale; Pacific Decadal Oscillation; temperature; teleconnection; time dependent intrinsic correlation

Received 26 February 2015; Revised 24 October 2015; Accepted 16 February 2016

1. Introduction

Global climate has been experiencing significant warming at an unprecedented pace in the past century (IPCC, 2013; Ji *et al.*, 2014). In the recent past, a large number of research works focused on this issue and attempted to study the variability of the Earth's surface temperature both at global and regional scales (Wu *et al.*, 2007, 2011; Hansen *et al.*, 2010; Capparelli *et al.*, 2013; Autret *et al.*, 2013; Bai *et al.*, 2015). Understanding the linkage of global surface temperature with different climate oscillations may help to obtain proper implications in regional-scale hydrology, under the climate change scenario. The effect of multi-decadal oscillations on the global surface temperature has been well debated in the literature (Pietrafesa *et al.*, 2013; Trenberth and Fasullo, 2013) and many studies have discussed the role of the Pacific Decadal Oscillation (PDO) (e.g. Trenberth and Hurrell, 1994; Trenberth *et al.*, 2007; Chen *et al.*, 2008; Trenberth and Fasullo, 2013). The Pacific Ocean appears to account for the majority of decadal variability, and events in the Pacific affect the Atlantic, Indian, and Southern Oceans as the system acts collectively to equilibrate changes in the flow of energy (Chen *et al.*, 2008). The warm and cold phases of the PDO influence surface warming differently; studies have found that while the warm phase of the PDO enhanced surface warming, the cold phase reduced it (Trenberth and Fasullo, 2013). Kosaka and Xie (2013) highlighted the role of the PDO in the apparent recent hiatus in global mean surface temperatures through an experiment on a climate model with radiative forcing and sea surface temperature (SST) over the central and eastern Pacific Ocean. The 1997–1998 El Niño event triggered a change from a warm (1976–1998) to cold (since 1999) (Trenberth and Fasullo, 2013) PDO phase. Thus, the realistic simulation of Pacific decadal variability is very important in global warming and climate change-related studies. Both the global surface temperature and climate oscillation (such as PDO) time series show non-linear, non-stationary, and multiscaling behaviour. Information on the association between PDO and Global Surface Temperature Anomaly (GSTA) in multiple time scales may allow realistic simulations of climate models, and

* Correspondence to: Adarsh Sankaran, Department of Civil Engineering, TKM College of Engineering, Kollam, Kerala 691005, India.
E-mail: adarsh.sankaran@yahoo.in

this study attempts to investigate the possible association between the two in a statistical perspective based on a robust spectral analysis technique.

Empirical mode decomposition (EMD) proposed by Huang *et al.* (1998), is a multiscale decomposition method that decomposes a time series signal into different modes called intrinsic mode functions (IMFs), each of which has a specific scale (periodicity) and governs some physical processes. The EMD process involves two steps: (i) identification of local extrema points and fitting the spline functions connecting them, and (ii) computing the mean series (of extrema) and finding a residue series (by subtracting the mean from the original series). The above process is known as 'sifting' and the sifting operation is iteratively continued till the resulting series become a zero mean series with the total number of extrema differing from the summation of number of local maxima and minima points at the most by one. The process is repeated till the final residue series is monotonic or contains only one peak. A detailed description of the EMD can be found in Rao and Hsu (2008). To overcome the 'scale mixing' problem of EMD, Wu and Huang (2005a) proposed a noise-assisted ensemble averaged procedure, namely, ensemble empirical mode decomposition (EEMD). This method has been successfully applied to analyze numerous climatic series (e.g. Huang and Wu, 2008; Qian *et al.*, 2011; Massei and Fournier, 2012; Qian and Zhou, 2014; Bai *et al.*, 2015). The obtained IMFs are the most appropriate inputs to perform the Hilbert transform, which may help to the study the spectral characteristics of non-linear and non-stationary time series in the time-frequency domain by finding instantaneous frequencies and amplitudes. Moreover, instantaneous frequencies are useful to obtain instantaneous periods that can be fixed as window sizes to perform a running correlation analysis called time-dependent intrinsic correlation (TDIC) while investigating the link between two non-linear and non-stationary time series signals. The objective of this study is to investigate the teleconnection between global surface temperature and the PDO in a multiscaling framework, employing TDIC analysis.

2. Methodology

The methodology used in this teleconnection involves the following steps:

- Decompose the two time series of concern with EEMD and identify the mean periodicity of IMFs.
- Perform cross-correlation between the IMFs.
- Apply Normalized Hilbert Transform with Direct Quadrature (NHT-DQ) (Huang *et al.*, 2009) to find instantaneous frequency (and hence instantaneous period).
- Employ the TDIC method to perform the multiscale running correlation between the IMFs of the two time series, using the instantaneous periods computed in step 3.

2.1. EEMD and the NHT-DQ scheme

EEMD involves (i) creating a pool of artificial signals by the addition of white noise series to the time series of concern; (ii) applying EMD upon each artificial signal to obtain different modes (of specific periodicity); and (iii) obtaining the ensemble average of each mode, which is considered to be the actual IMF by EEMD decomposition. More details on EEMD can be found in Wu and Huang (2005a). The IMFs obtained are then subjected to Hilbert transformation (HT), to obtain instantaneous frequencies and amplitudes to study the spectral properties of the time series. To avoid the possibility of obtaining negative instantaneous frequencies (which are physically meaningless) and to ensure mathematical correctness of the transformation, Huang *et al.* (2009) proposed a normalization scheme for HT [normalized HT (NHT) and a direct quadrature (DQ)] variant of Hilbert transform. The normalization scheme primarily involves (i) identification of the local maxima of IMF series; (ii) spline fitting through maxima points; and (iii) point by point division of IMFs using the constructed spline. The third step is repeated iteratively until the normalized maximum values are all unity. The final series will be the frequency modulated (FM) part that helps determine the amplitude modulated (AM) part of the signal. This normalization process and the application of Hilbert transform to the empirical AM signal form the NHT method and the use of '*arccosine*' instead of the '*arctan*' in the computation of phase angles makes the scheme DQ. More details of the scheme can be found in Huang and Wu (2008) or Huang *et al.* (2009). This study uses the NHT-DQ scheme to find instantaneous frequencies required to perform TDIC analysis.

2.2. TDIC analysis

Because most of the hydro-climatic time series possess multiscaling behaviour, a scale-dependent running correlation analysis is more appropriate to establish multiscale teleconnections of climate variables (Papadimitriou *et al.*, 2006; Rodo and Rodriguez-Arias, 2006; Scafetta, 2014). However, the selection of an appropriate window size is a challenge while applying such techniques. Chen *et al.* (2010) proposed a method to determine the scale-dependent correlation between two time series, namely, the TDIC. This method employs the EMD (or its variants) to decompose both the time series data into multiple time scales. It is to be noted that in this method, the window size is fixed adaptively (based on the data characteristics), keeping the stationarity property of the data within the window and, more importantly, the size of the sliding window is fixed based on the instantaneous period (computed from instantaneous frequencies obtained by HT of IMFs). The different steps of the TDIC analysis are given below:

1. Use EMD (or its variants) to decompose the two time series of interest into different time scales.

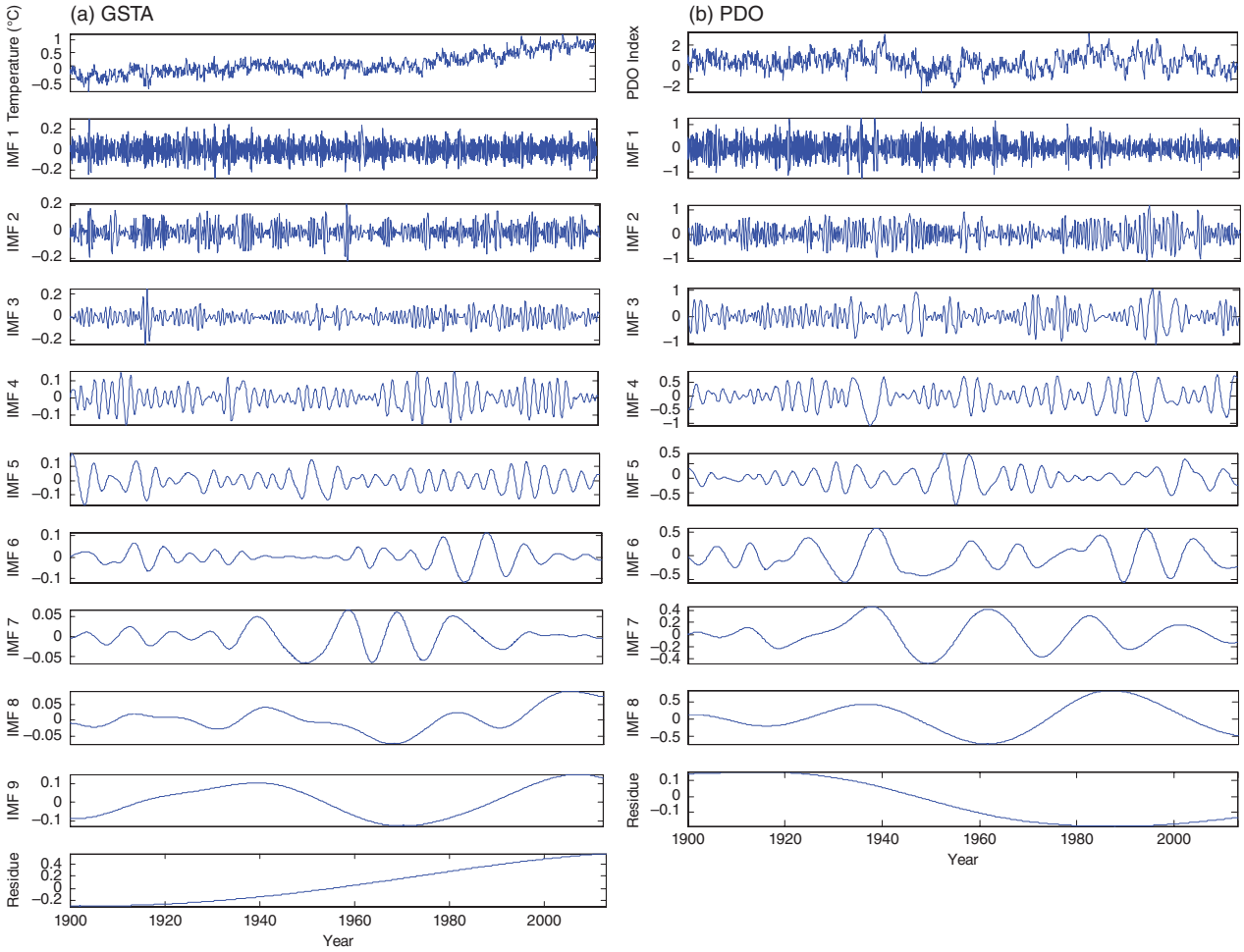

Figure 1. IMFs of monthly GSTA and PDO time series for the period 1901–2013.

2. Compare the mean periodicities of the IMFs of both series and select those IMFs with nearly the same mean periodicity.
3. Find the instantaneous periods of both the IMFs using Hilbert transform.
4. Find the minimum sliding window size (t_d), which may be taken as the maximum instantaneous period between the two signals at the current position t_k, i.e. $t_d = \max(T_{1,i}(t_k), T_{2,i}(t_k))$, where $T_{1,i}$ and $T_{2,i}$ are instantaneous periods.
5. Fix the sliding window as $t_w^n \left[t_k - \frac{nt_d}{2} : t_k + \frac{nt_d}{2} \right]$, where n is any positive number (a multiplication factor for minimum sliding window size). In this study, n is taken as 1, following previous studies (Huang and Schmitt, 2014).
6. Assume that IMF1 and IMF2 are two IMFs of nearly the same mean period pertaining to the two different time series. The TDIC of the pair of IMFs can be estimated from

$R_i\left(t_k^n\right) = \mathrm{Corr}\left(\mathrm{IMF}_{1,i}\left(t_w^n\right), \mathrm{IMF}_{2,i}\left(t_w^n\right)\right)$ at any t_k, where Corr is the correlation coefficient of the two time series and $R_i(t_k{}^n)$ is the correlation coefficient between the two IMF segments at current position.

7 Perform Student's t-test to investigate whether the correlation coefficient $R_i\left(t_k^n\right)$ is statistically significant.
8 Repeat steps 4 to 7 iteratively till the boundary of the sliding window exceeds the end points of the time series.

After computing the TDIC matrix, the TDIC plot is prepared. The horizontal axis of the TDIC plot is the time of the series (corresponding to the centre position of the sliding window), and the vertical axis is the size of the sliding window. The TDIC plot will be triangular in shape, and the correlation at the apex point will be the general correlation coefficient between the series if the data length is fixed as maximum size of sliding window (Chen *et al.*, 2010). In general, half of the data length is selected as the maximum size of the sliding window. The bottom contour of the TDIC plots depicts the instantaneous frequency, and hence a shift of the plots to larger time scales can be noticed in higher-order IMFs (i.e. of low-frequency modes).

3. Database

PDO is described as a long-lived El Niño-like pattern of Pacific climate variability (Mantua *et al.*, 1997; Zhang *et al.*, 1997), which can be determined by projecting the

SST anomaly on the leading empirical orthogonal functions (EOFs) of monthly SST anomaly in the northern Pacific Ocean. To investigate the link between global surface temperature and the PDO, the monthly PDO indices for the period 1901–2013 are collected from the Joint Institute for the Study of the Atmosphere and Ocean (JISAO) (http://jisao.washington.edu/pdo/PDO.latest) and the GSTA data collected from National Aeronautics and Space Administration (NASA) (http://data.giss.nasa.gov/gistemp/tabledata_v3/GLB.Ts.txt).

4. Results and discussion

This study uses the EEMD method to decompose the PDO and GSTA series after adopting a noise standard deviation of 0.2 and ensemble size of 100 (Bai *et al.*, 2015). For the GSTA series, the decomposition resulted in nine IMFs and a residue. The modes obtained by the decomposition are presented in Figure 1, and the mean periodicity of different modes estimated using the zero-crossing method (Barnhart and Eichinger, 2011) and the percentage variability explained (Bai *et al.*, 2015) by different modes are presented in Table 1.

Because the EEMD is a noise-assisted data analysis method, where white noise series is added to form artificial signals, the spurious time scales may be introduced and this may lead to wrong or misleading interpretations in the TDIC analysis. Therefore, before drawing useful inferences from the modes obtained from decomposition, it is important to ensure that the resulting modes are not from the added noise. The statistical significance test of IMF components (Wu and Huang, 2004, 2005b) can be used to identify the significant modes of decomposition and eliminate the noisy components from the time series. Basically, this involves (i) computation of the energy density of IMFs and its normalization by considering the first IMF as the reference IMF; (ii) generation of a white noise series by Monte Carlo simulations, as well as its EMD, and computation of the 'spread function'; and (iii) estimation of the confidence band of spread function of white noise at a selected significance level based on step (ii). The coordinate points of mean normalized energy and mean period of IMFs are located on the 2D plane. This allows comparison of the energy level of different IMFs with the spread function of white noise. The IMFs of the original time series $X(t)$ that have their energy densities located above the upper confidence line of the white noise series can be considered the 'true IMFs' (free from white noise and containing information) and statistically significant at the selected confidence level. Complete details of the statistical significance test of the IMF component can be found in Wu and Huang (2004, 2005b). The results of statistical significance tests of the IMF components of the GSTA and PDO time series are presented in Figure 2. From Figure 2, it is clear that the different modes are above the upper confidence lines and hence free from noise.

The decomposition resulted in the detection of intra-annual cycles of ∼3 and ∼6 months, a near-annual periodicity (∼11–13 month periodicity), three inter-annual modes, a decadal mode (∼124-month periodicity), and two inter-decadal modes. The residue represents the slowly varying climate component and the decomposition detected the well-established monotonically increasing trend of the GSTA dataset (Wu *et al.*, 2007, 2011; Barnhart and Eichinger, 2011; Lee and Ourada, 2011; Franske, 2014). The near-decadal periodicity observed in the decomposition of GSTA (∼124 months) could be associated with the ∼11-year sunspot cycles; this link has been proven in earlier studies (Usoskin and Mursula, 2003; Coughlin and Tung, 2004; Zhen-Shan and Xian, 2007; Barnhart and Eichinger, 2011). The decomposition of PDO resulted in eight IMFs and a residue. Table 1 further shows that for the GSTA dataset, the maximum variability is explained by the trend (residue) component (∼71%) followed by IMF1 and IMF2. This might be attributed to the consistently increasing nature of the GSTA dataset. Similar results were also reported in earlier research works (Lee and Ourada, 2011). However, for the PDO time series, the variability is explained mainly by the first five modes and the eighth mode (∼10–18%). From Table 1, we find that the periodicity of both GSTA and PDO matches reasonably well, particularly for lower modes; however, larger differences in periodicities (scales) are observed for the low-frequency IMFs (eighth and ninth modes). This implies that exactly common scales did not present in both the series at some of the larger modes, probably because of the limited number of cycles in the higher-order IMFs. We also found that the periodicity of the residue is long term, and it is denoted as 1356 (length of the dataset) for illustration purposes. The slowly varying residue component depicts the overall inherent trend in the data; however, it is to be noted that a mere comparison of the residue (non-stationary component) is not sufficient to comment on the association between the two time series, as the trend depends on the length of the dataset chosen. Therefore, to examine the association between the two time series, we perform a cross-correlation analysis of the series' IMFs at different process scales; the results are presented in Table 2.

Table 1. Periodicity of IMFs of GSTA and PDO time series and percentage of variability explained by different modes.

Mode number	GSTA		PDO	
	Time period (months)	% Variability explained	Time period (months)	% Variability explained
IMF1	2.8	7.26	2.9	17.78
IMF2	5.7	3.25	5.5	12.67
IMF3	10.5	2.18	10.6	11.94
IMF4	20.2	2.85	20.0	14.88
IMF5	43.7	3.65	42.9	10.67
IMF6	67.8	1.16	73.1	5.98
IMF7	123.3	0.76	124.3	6.40
IMF8	271.2	1.28	414.3	17.62
IMF9/residue	678	6.21	1356	2.06
Residue	1356	71.37		

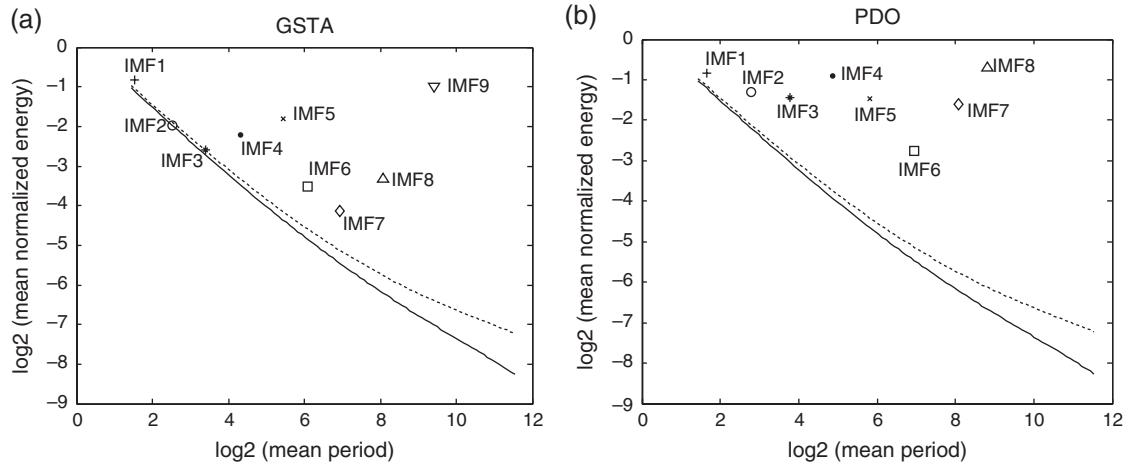

Figure 2. Statistical significance test for IMF components of GSTA and PDO series with 95% (solid line) and 99% (dotted line) confidence limits. The IMFs certainly do not result from noise considering that the energy levels of different IMFs are above the upper confidence limits.

Table 2. Cross-correlation between IMFs of GSTA and PDO time series.

PDO	Temperature									
	IMF1	IMF2	IMF3	IMF4	IMF5	IMF6	IMF7	IMF8	IMF9	Residue
IMF1	0.041	0.049	0.026	−0.024	−0.031	0.000	−0.010	0.004	−0.007	0.011
IMF2	0.020	−0.050	0.038	0.013	0.029	−0.027	0.001	−0.001	0.009	−0.024
IMF3	−0.018	−0.001	−0.057	0.054	0.010	0.009	−0.031	−0.004	0.012	0.001
IMF4	0.006	0.016	−0.015	**0.131**	**0.102**	−0.013	−0.076	−0.052	−0.051	−0.003
IMF5	−0.006	−0.014	0.004	0.043	**0.421**	0.012	−0.030	0.031	0.034	0.029
IMF6	−0.014	−0.011	0.001	0.031	0.075	**−0.137**	**0.518**	**0.107**	−0.068	0.069
IMF7	0.007	−0.028	0.006	0.032	0.045	−0.030	**0.545**	0.076	0.018	−0.031
IMF8	−0.007	0.014	0.000	0.012	0.001	−0.044	0.068	**0.132**	**0.160**	0.158
Residue	0.000	−0.004	−0.011	0.027	0.026	0.015	−0.020	−0.066	**0.118**	**−0.921**

The bold figures indicate that the correlation coefficient is significant (p value <0.00001).

From Table 2, we note that the association between the respective IMFs at different process (time) scales is not unique; that is, the correlation between the corresponding IMFs are positive at some scales (IMF1, IMF4, IMF7, and IMF8) and negative at some other time scales (IMF2, IMF3, and IMF6). However, the correlation between the residues is negative (and statistically significant). We further note that the magnitude of correlation between the different IMFs is very small except for the residue component (−0.921). The overall linear correlation between the GSTA and PDO series is only 0.054 when we consider the entire time span. The reason for this very low correlation could be that the positive correlation at some process scale might have been nullified by a negative correlation at some of the other scales; similarly, within a particular IMF, the positive correlation at some of the time spells might have been nullified by a negative correlation at some other time spells. This observation is remarkable, as it leads to the conclusion that the association between the two time series is not always of unique nature. To verify this hypothesis, we present a plot of the first seven IMFs (in which a matching in mean periodicity is observed) and the residue in Figure 3.

A close inspection of the IMF pairs (different panels of Figure 3) showed several time spells with similar evolution of IMFs (e.g. 1981–2001 in IMF7 and 1970–1980 in IMF5). However, in some of the shorter time spells, the evolution is dissimilar in characteristics (e.g. 1981–2001 in IMF6) or very weak in association (e.g. weak PDO prior to 1921 in IMF4 and during 1941–1961 in IMF6). Some shorter time spells show a shift in phase between the two series (e.g. during 1961–1981 in IMF7). Further, we noticed that a zero crossing of PDO occurs in the 1950s and a zero crossing of GSTA occurs in 1960 (from the last panel), indicating a similar evolution of the non-stationary component below and above the zero mean. This observation highlights the importance of a running correlation analysis to detect such unusual relationships at local time spells. Thus, the hypothesis of the alterative nature of correlation is found to be correct from a visual examination of the IMFs as localized differences in the nature of the association of IMFs are clearly evident in the time domain.

To quantify such local associations (i.e. to detect such correlations of opposing character), a dynamic correlation analysis (Rodo and Rodriguez-Arias, 2006; Scafetta, 2014) needs to be performed. The traditional correlation analysis depicts the linear association between two series by assuming their stationarity. While investigating the association between two time series of multiscaling character through a running correlation

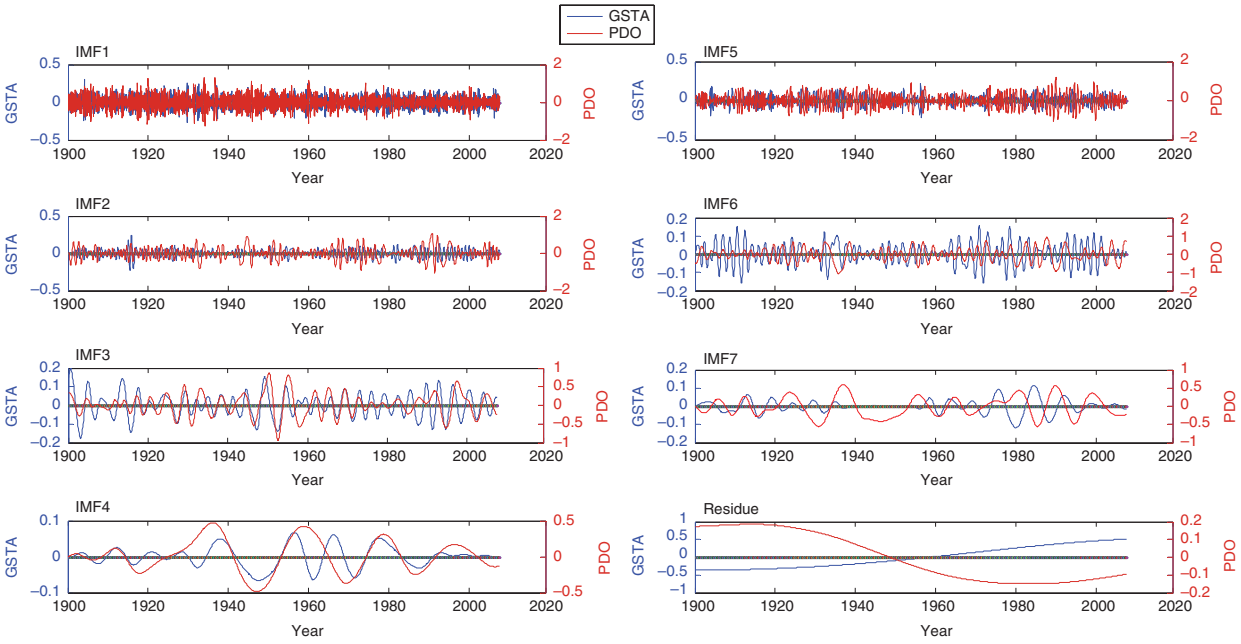

Figure 3. Comparison of different modes of monthly GSTA and PDO time series for the period 1901–2013.

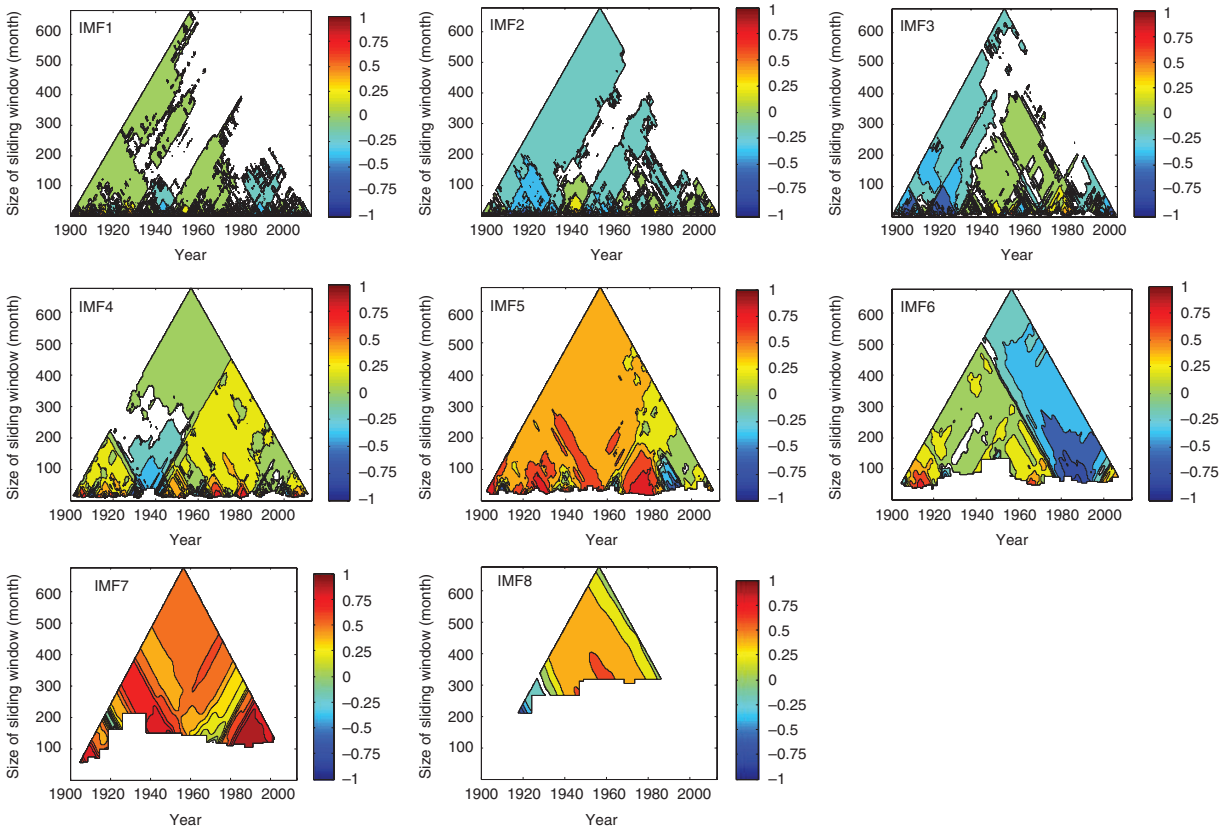

Figure 4. TDIC plots between IMF of PDO and that of GSTA time series for the period 1901–2013 at different process scales. The white space indicates that the correlation is not significant at the 5% level using Student's *t*-test.

analysis, we need to ensure the stationarity property within the sliding window rather than over the entire time domain. These issues can be successfully addressed by using the TDIC method propounded by Chen *et al.* (2010). TDIC analysis is performed between IMFs of comparable periodicity from two time series. Here, the sliding window is selected adaptively after finding instantaneous frequencies by the NHT-DQ scheme of the selected IMF pair. The results of the TDIC analysis are presented in Figure 4.

Table 3. Periodicity of IMFs of GSTA and PDO series for different time span.

IMF number	Time period (months)									
	Cold phase 1 (CP1)		Warm phase 1 (WP1)		Cold phase 2 (CP2)		Warm phase 2 (WP2)		Recent past (RP)	
	GSTA	PDO	GSTA	PDO	GSTA	PDO	GSTA	PDO	GSTA	PDO
IMF1	2.9	3.0	3.0	3.1	3.1	3.1	2.9	3.3	2.9	3.3
IMF2	5.6	5.9	6.4	8.0	6.5	6.7	6.6	8.8	6.8	8.0
IMF3	11.5	13.1	11.0	14.7	13.3	12.4	12.0	12.8	11.4	13.4
IMF4	26.2	28.8	24.0	33.0	32.7	27.7	25.3	38.0	27.0	30.8
IMF5	57.6	57.6	44.0	52.8	60.0	60.0	38.0	76.0	43.2	72.0
IMF6	96.0	96.0	132.0	88.0	180.0	120.0	114.0	154.0	216.0	216.0
IMF7/ Residue	288.0	288.0	264.0	132.0	360.0	180.0	228.0	228.0	216.0	
				264.0		360.0				

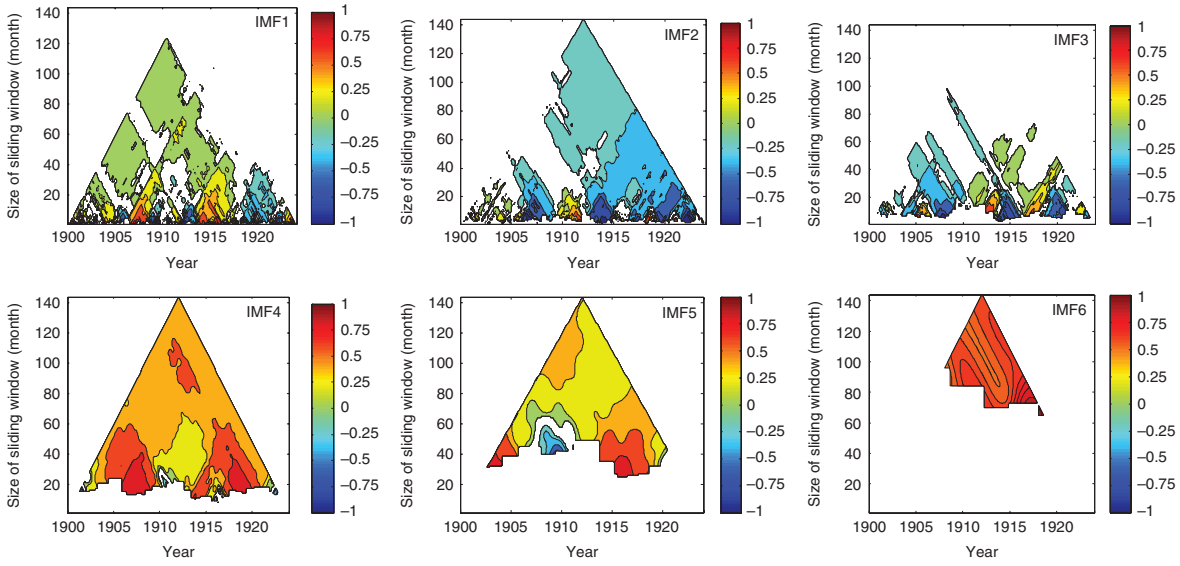

Figure 5. TDIC plots between IMF of PDO and that of GSTA time series of the first cold PDO phase of the 20th century (1901–1924) at different process scales. The white space indicates that the correlation is not significant at the 5% level using Student's *t*-test.

The TDIC plots show an overall long-range correlation between the PDO and GSTA in most of the modes. A careful perusal of Figure 4 shows a pattern of correlation quite unstable for the first few high-frequency modes (IMF1–IMF4) and rich dynamics in the nature of correlation, particularly at lower time scales (e.g. for sliding window size <100 months). That is, although the dominance of negative correlation is noticed in the TDIC plots of lower-order IMFs, a large number of shorter time spells appear where a positive correlation between the two exists. This 'switching' in the nature of correlations is more visible in IMF4 as the time window is of the order of a few years (alternate red and blue/green colour shades in the TDIC plot of IMF4), whereas alterations in nature of correlations last only for few months (i.e. frequent reversals) in IMF1–IMF3. The pattern of correlation is quite stable in the other IMFs, with the presence of only a few localized couplets (opposing nature of correlations). The TDIC plots of IMF5 show a long-range positive correlation for IMF5, but we notice a localized negative correlation between the two in the 1990s. Similarly, the association between IMF6 of GSTA and PDO is primarily negative, but a strong positive correlation exists for the decade prior to 1920. IMF7 is of a decadal scale; for IMF7, there exists a strong long-range positive correlation. For IMF8 (inter-decadal scale exceeding a ~20-year periodicity), the two series show strong positive correlation with no reversals in the nature of association.

4.1. TDIC analysis for different PDO phases

Next, we perform another set of TDIC analyses, considering the time series of the cold (1901–1924, 1947–1976) and warm (1925–1946 and 1977–1995) phases of the PDO in the 20th century as well as the GSTA time series for the recent past (1995–2013). The mean IMF periodicities of the GSTA and PDO for different cases are presented in Table 3.

The periodicities of IMFs obtained from the decomposition of the GSTA and PDO series for five different periods (Cold Phase 1-CP1, Warm Phase 1-WP1, Cold Phase 2-CP2, Warm Phase 2-WP2, and Recent Past-RP) are presented in Table 3. The decomposition resulted in two intra-annual modes (IMF1, IMF2), an annual mode (IMF3), and three inter-annual modes (IMF4–IMF6) for

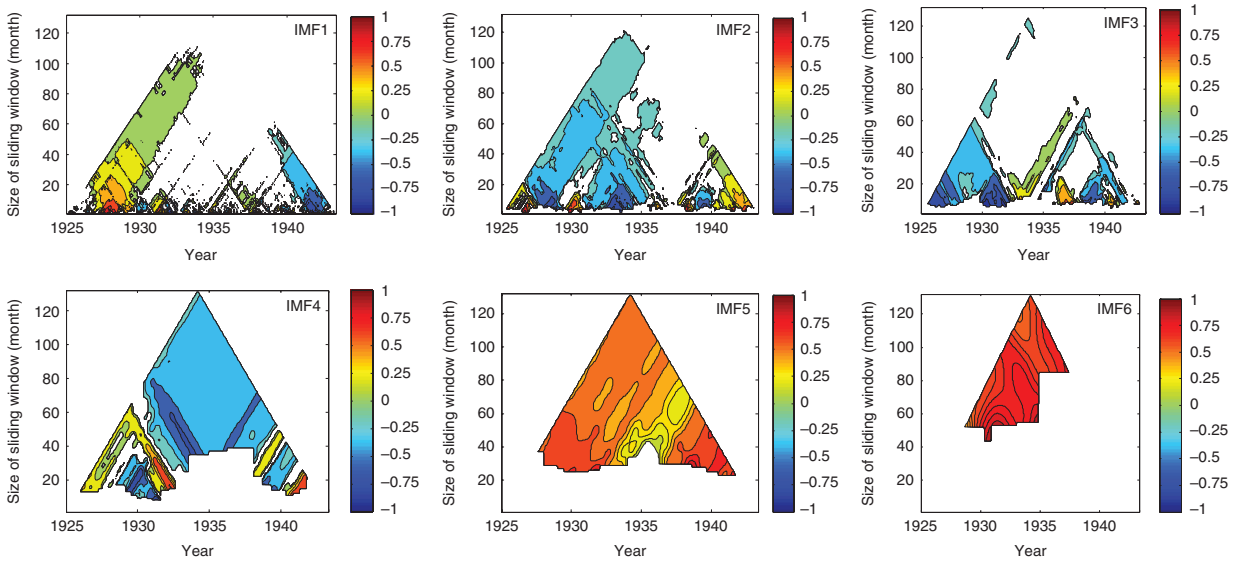

Figure 6. TDIC plots between IMF of PDO and that of GSTA time series of the first warm PDO phase of the last 20th century (1925–1946) at different process scales. The white space indicates that the correlation is not significant at the 5% level using Student's *t*-test.

all cases. Table 3 further shows that the periodicity of the GSTA and PDO matches fairly well, particularly for lower-order modes.

The TDIC plot for the CP1 period is presented in Figure 5. From Figure 5 it is noticed that, for lower-order IMFs (IMF1-IMF3), the correlation between the series is primarily weakly negative, but a strong positive correlation prevails for some of the periods (1907–1908 and 1914–1916 in IMF1, 1911–1912 in IMF2, etc.). For IMF3, the correlation between the series is not statistically significant for longer sliding window sizes (i.e. they show significant correlations only at shorter ranges). For IMF4 (of ∼2-year periodicity), a strong long-range positive correlation exists between PDO and GSTA. Similarly, a strong positive correlation between the series exists in most scales for most of the period for IMF5; in IMF6, the correlation does not 'switch over' to negative.

TDIC plots of different IMFs for the PDO of the first warm phase of the 20th century (1925–1946) and GSTA are presented in Figure 6. The association between the series is primarily weakly negative for the first three IMFs. Correlation between the IMFs is strongly negative for IMF4 (∼2.5-year periodicity) at most of the scale ranges and strongly positive for IMF5 and IMF6. The TDIC analysis of IMFs of these time series pairs also detects a transition in nature of correlations from positive to negative (or vice versa) at many short-term time spells and scale ranges except for IMF6.

To check for evidence of any change in the overall pattern of correlations among the different PDO phases, similar analyses are performed for the other three time spells – the cold phase of 1947–1976 (CP2), the warm phase of 1977–1995 (WP2), and the recent past (RP) (1996–2013); the results are presented in Figures 7–9, respectively. Interestingly, a comparison of Figures 5 and 7 shows that the pattern of correlations at different process scales (i.e. for different IMFs) is quite similar for both cold phases. The TDIC analysis of IMFs of CP2 also detected its strong long-term association with GSTA in IMF4 (of ∼2–3-year periodicity). However, from Figure 8, we find that for warm phase 2 (1977–1995), the statistical significance of the correlations of different IMFs is more localized (with more void spaces in the TDIC plot) and the pattern of correlation is quite different from that for the first warm phase period (1925–1946) (Figure 6). The recent past (1996–2013) is also a cold phase; a strong long-term positive association between PDO and GSTA is noticed at IMF4 for the ∼2.5-year periodicity (Figure 9). Note that in all plots, we find frequent reversals in the nature of correlation, but the time scale (*y*-axis of TDIC plot) and period for which a particular pattern of correlation persists vary with IMFs.

This article contributed an investigation on the multiscale teleconnection between the PDO and global surface temperature. Some remarkable observations made from the study are: (i) the nature of association between PDO and global surface temperature varies with time scales and is dynamic within the time domain; (ii) a positive association between GSTA and PDO may gets displayed even at intra-decadal time scales; (iii) the pattern of correlation between GSTA and PDO can be different in cold and warm phase of PDO; (iv) even during two different episodes of same PDO phase, the pattern of correlation between GSTA and PDO can be different; (v) there exists frequent reversals in the nature of association between GSTA and PDO over the time domain and time scale. Broad inferences and possible reasons behind such observations can be deduced from the study. It is well understood that external or internal climatic forcings (such as natural variations in cloud, aerosols, changes in sunspot and solar irradiance, volcanic eruptions, and oceanic heating/cooling) are responsible for global surface temperature changes. External physical mechanisms operating at different time scales and local perturbations may result in

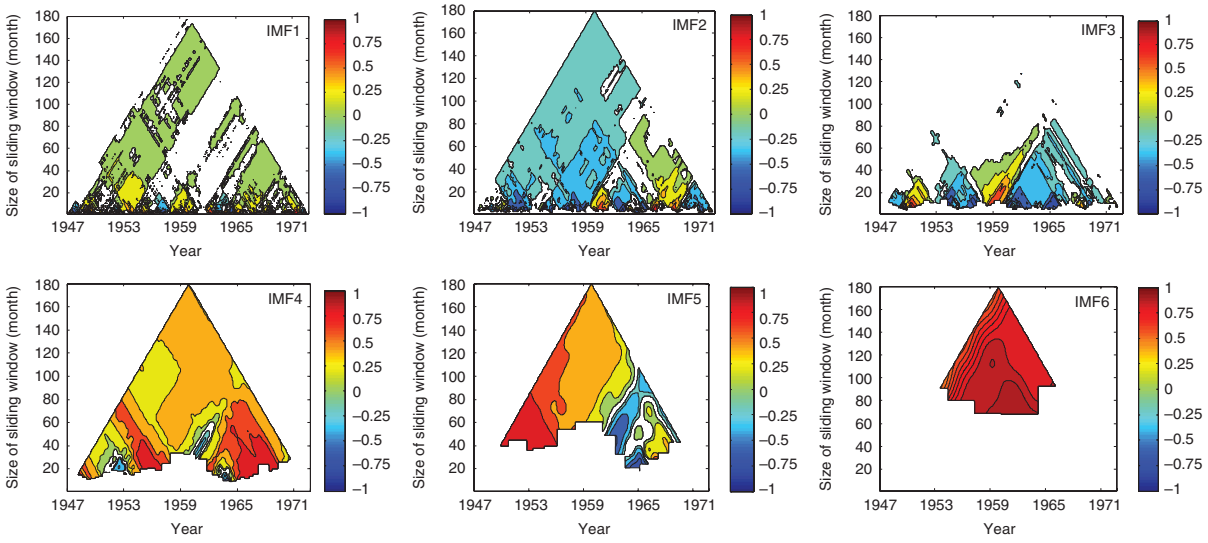

Figure 7. TDIC plots between IMF of PDO and that of GSTA time series of the second cold PDO phase of the 20th century (1947–1976) at different process scales. The white space in the plot indicates that the correlation is not significant at the 5% level using Student's *t*-test.

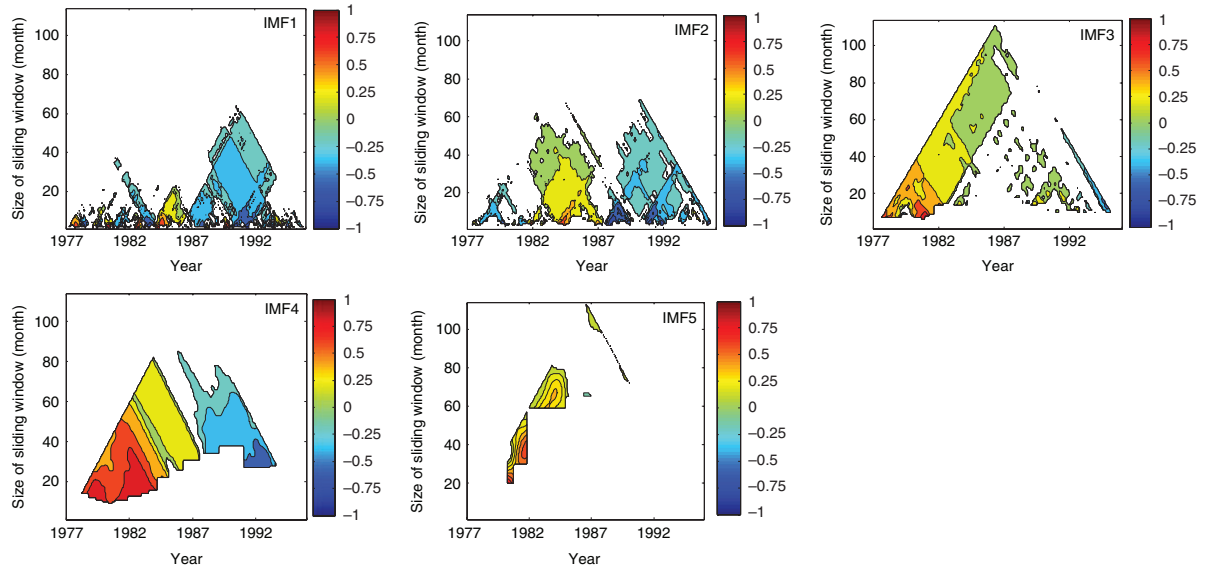

Figure 8. TDIC plots between IMF of PDO and that of GSTA time series of the second warm PDO phase of the 20th century (1977–1995) at different process scales. The white space indicates that the correlation is not significant at the 5% level using Student's *t*-test.

natural variability, such as the PDO. Even if the influence of external forcing on the GSTA and PDO remains similar, internal factors may show regional differences. This may be the reason behind the display of different correlation patterns at different time scales while investigating the association of global surface temperature with the PDO. However, the pattern of correlation between the PDO and GSTA may differ during the warm phase and cold phases of PDO because of the difference in responsible factors for PDO/GSTA during the different PDO phases. It is now implicit that, how the global surface temperature gets manifested primarily depends on amount of energy gets sequestrated within ocean. The energy gets transferred to the deep ocean during the cold PDO phases eventually leads to a cooler surface (and vice versa during the warm PDO phase). Such oceanic heating/cooling can influence the GSTA–PDO associations. The recovery of such energy loss may take several years (e.g. ∼25 years), and such effects are therefore more perceptible at the decadal/inter-decadal scale. Thus, the positive association between the two is perceptible at longer process scales (i.e. in low-frequency modes) and if some of the localized factors catalyze the process, a positive association may be displayed in intra-decadal modes. Interestingly, the pattern of correlation between GSTA and PDO is found to be similar during the two cold PDO phases of the past century, whereas it is found to be different during the two warm phases of the past century. Again in the recent past period, it shows a completely different pattern. This difference in the pattern of correlation in different episodes of the same phase might be due to the differences in global temperature or the energy content received by the

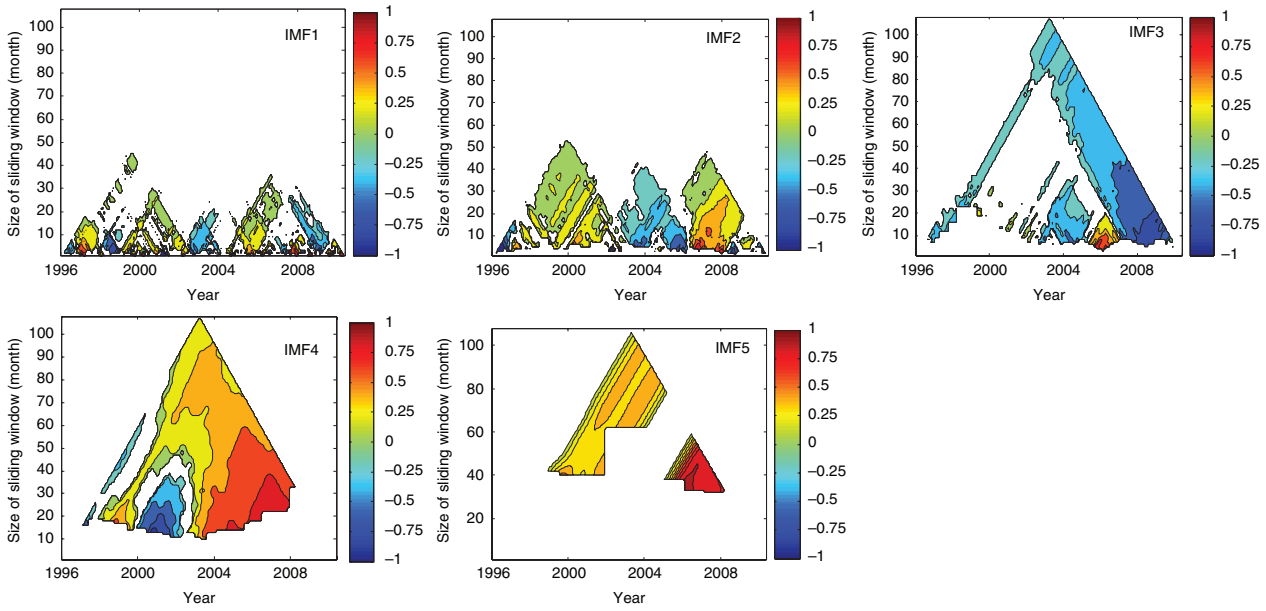

Figure 9. TDIC plots between IMF of PDO and that of GSTA time series of the recent past (1996–2013) at different process scales. The white space indicates that the correlation is not significant at the 5% level using Student's *t*-test.

oceans during the different episodes of same phase. Here the different possibilities are: (i) the amount of energy received by the ocean differs during the two warm (or cold) phases while the global temperature remains same; (ii) although the amount of energy content received by the ocean during two warm phases (or cold phases) remains the same, some of the factors responsible for temperature changes (such as aerosol content, CO_2 concentration) might have resulted in a different picture of energy imbalance at the top-of-atmosphere (TOA); (iii) both the quantity of energy transfer and the global temperature might differed during two different warm (or cold) phases of PDO. Due to any of the above reason, the strength of association between GSTA and PDO (depicted by the pattern of correlation) differs. Identifying the exact reason behind the switching of nature of correlations – either the physical processes governing such changes or the interaction between different climate forcings (Trenberth and Fasullo 2013; Wang *et al.*, 2014) remains an open scientific problem that needs to be investigated in a subsequent study.

5. Conclusions

This study deduced broad inferences on the multiscale association between GSTA with PDO using the EEMD and TDIC methods. The important conclusions of the study are as follows:

(i) The periodicities of different PDO and GSTA modes show close matching for lower modes and a cross-correlation analysis between the IMFs of GSTA and PDO showed that linear association of modes is the most perceptible at the slowly varying trend component.

(ii) PDO and GSTA are related in multiple time scales, and their relationship is not unique in both time scale and time domain. A positive relation may prevail between the two at certain time spells and scales, whereas a contrasting behaviour may occur at other time spells and scales. There could be a multitude of such couplets of contrasting correlations, especially in high-frequency modes. Although the obvious reasons for such 'switchovers' in the nature of correlation cannot be adduced at the present stage, such transitions may be attributed to some unidentified physical processes, spatial non-homogeneity, or inter-relationships between different climate forcings. Further investigation may be necessary to corroborate this observation.

(iii) A strong and significant long-range positive correlation is observed between GSTA and PDO for decadal and inter-decadal modes exceeding (∼) 20-year periodicities, and the correlations between the two are consistent at this time scale; that is, for the modes of these time scales, there are less-frequent reversals of correlations compared with that at other time scales.

(iv) A similar pattern of correlations is observed for both cold phases of the 20th century (1901–1924 and 1947–1976) at different process scales. However, the pattern of correlation for different process scales is different for the warm PDO phases (1925–1946 and 1977–1955).

Acknowledgements

The author expresses his sincere gratitude to Dr Radan Huth, editor of the journal, and two anonymous reviewers for their help in improving the quality of the manuscript considerably through constructive comments. The author

offers his special and sincere thanks to Prof. Francois G. Schmitt, Director, Laboratory of Oceanology and Geosciences (LOG), University of Lille, Wimereux, France, for the scientific discussions on the HHT and TDIC methods during his visit to the LOG in October 2014. The author also thanks Dr. Yong Xiang Huang of the Shanghai Institute of Applied Mathematics and Mechanics, Shanghai University, Shanghai, China, for providing the basic source code for TDIC analysis in the MATLAB platform at the website http://zenodo.org/record/9748?ln=en for the promotion of non-commercial scientific research.

References

Autret G, Remy F, Roques S. 2013. Multiscale analysis of Antarctic surface temperature series by empirical mode decomposition. *J. Atmos. Ocean. Technol.* **30**: 649–654.

Bai L, Xu J, Chen Z, Li W, Liu Z, Zhao B, Wang Z. 2015. The regional features of temperature variation trends over Xinjiang in China by the ensemble empirical mode decomposition method. *Int. J. Climatol.* **35**(11): 3229–3237.

Barnhart BL, Eichinger WE. 2011. Empirical mode decomposition applied to solar irradiance, global temperature, sunspot number and CO_2 concentration data. *J. Atmos. Sol.-Terr. Phys.* **73**: 1771–1779.

Capparelli V, Franzke C, Vecchio A, Freeman MP, Watkins NW, Carbone V. 2013. Spatio-temporal analysis of U.S. station temperature trends over the last century. *J. Geophys. Res. Atmos.* **118**(14): 7427–7434, doi: 10.1002/jgrd.50551.

Chen J, Del Genio AD, Carlson BE, Bosilovich MG. 2008. The spatio-temporal structure of twentieth-century climate variations in observations and re-analyses. Part II: Pacific pan-decadal variability. *J. Clim.* **21**: 2634–2650.

Chen X, Wu Z, Huang NE. 2010. The time-dependent intrinsic correlation based on the empirical mode decomposition. *Adv. Adapt. Data Anal.* **2**: 233–265.

Coughlin K, Tung KK. 2004. Eleven-year solar cycle signal 665 throughout the lower atmosphere. *J. Geophys. Res.* **109**(D21105): 666, doi: 10.1029/2004JD004873.

Franske CL. 2014. Non-linear climate change. *Nat. Clim. Change* **4**: 423–424.

Hansen J, Ruedy R, Sato M, Lo K. 2010. Global surface temperature change. *Rev. Geophys.* **48**: RG4004.

Huang Y, Schmitt FG. 2014. Time-dependent intrinsic correlation analysis of temperature and dissolved oxygen time series using empirical mode decomposition. *J. Mar. Syst.* **130**: 90–100.

Huang NE, Wu Z. 2008. A review on Hilbert Huang Transform: method and its applications to geophysical studies. *Rev. Geophys.* **46**(2): RG2006, doi: 10.1029/2007RG000228.

Huang NE, Shen Z, Long SR, Wu MC, Shih HH, Zheng Q, Yen NC, Tung CC, Liu HH. 1998. The empirical mode decomposition and the Hilbert spectrum for nonlinear and non-stationary time series analysis. *Proc. R. Soc. Lond. B Biol. Sci. Ser. A* **454**: 903–995.

Huang NE, Wu Z, Long SR, Arnold KC, Blank K, Liu TW. 2009. On instantaneous frequency. *Adv. Adapt. Data Anal.* **1**(2): 177–229.

IPCC. 2013. *Climate Change 2013: The Physical Science Basis*. Cambridge University Press: Cambridge, UK.

Ji F, Wu Z, Huang J, Chasseignet EP. 2014. Evolution of land surface air temperature trend. *Nat. Clim. Change* **4**: 462–466.

Kosaka Y, Xie SP. 2013. Recent global-warming hiatus tied to equatorial Pacific surface cooling. *Nature* **501**: 403–407.

Lee T, Ourada TBMJ. 2011. Prediction of climate non-stationary oscillation processes with empirical mode decomposition. *J. Geophys. Res.* **116**: D06107, doi: 10.1029/2010JD015142.

Mantua NJ, Hare SR, Zhang Y, Wallace JM, Francis R. 1997. A Pacific inter-decadal climate oscillation with impacts on salmon production. *Bull. Am. Meteorol. Soc.* **78**: 1069–1079.

Massei N, Fournier M. 2012. Assessing the expression of large-scale climatic fluctuations in the hydrologic variability of daily Seine river flow (France) between 1950 and 2008 using Hilbert Huang Transform. *J. Hydrol.* **448–449**: 119–128.

Papadimitriou S, Sun J, Yu PS. 2006. Local correlation tracking in time series. In *Proceedings of Sixth International Conference on Data Mining*, IEEE Computer Society, Washington, DC, 456–465.

Pietrafesa LJ, Dickey DA, Gayes PT, Yan T, Epps JM, Hagan M, Bao S, Peng M. 2013. On atmospheric-oceanic-land temperature variability and trends. *Int. J. Geosci.* **4**: 417–443.

Qian C, Zhou T. 2014. Multidecadal variability of North China aridity and its relationship to PDO during 1900–2010. *J. Clim.* **27**(3): 1210–1222.

Qian C, Wu Z, Fu C, Wang D. 2011. On changing El Niño: a view from time-varying annual cycle, inter-annual variability and mean state. *J. Clim.* **24**(24): 6486–6500.

Rao AR, Hsu EC. 2008. *Hilbert Huang Transform Analysis of Hydrological and Environmental Time Series*. Springer Verlag: Dordrecht, The Netherlands.

Rodo X, Rodriguez-Arias MA. 2006. A new method to detect transitory signatures and local time/space variability structures in the climate system: the scale-dependent correlation analysis. *Clim. Dyn.* **27**(5): 441–458.

Scafetta N. 2014. Multi-scale dynamical analysis (MSDA) of sea level records vs. PDO, AMO, and NAO indexes. *Clim. Dyn.* **43**: 175–192.

Trenberth KE, Fasullo JT. 2013. An apparent hiatus in global warming? *Earth's Future* **1**: 19–32.

Trenberth KE, Hurrell JW. 1994. Decadal atmosphere–ocean variations in the Pacific. *Clim. Dyn.* **9**: 303–319.

Trenberth KE , Jones PD, Ambenje P, Bojariu R, Esterling D, Klein Tank A, Parkaer D, Rahimzadeh F, Renwick JA, Rusticucci M, Soden B, Zhai P. 2007. Observations: surface and atmospheric climate change. In *Climate Change 2007. The Physical Science Basis*, Solomon S, Qin D, Manning M, Chen Z, Marquis M, Averyat KB, Tignor M, Miller HL (eds). Cambridge University Press: Cambridge, UK, 235–336.

Usoskin IG, Mursula K. 2003. Long-term solar cycle evolution: review of recent developments. *Sol. Phys.* **218**: 319–343.

Wang S, Huang J, He Y, Guan Y. 2014. Combined effects of the Pacific Decadal Oscillation and El Niño-Southern Oscillation on global land dry-wet changes. *Nat. Clim. Change* **4**: 6651, doi: 10.1038/srep06651.

Wu Z, Huang NE. 2004. A study of the characteristics of white noise using the empirical mode decomposition method. *Proc. R. Soc. Lond. Ser. A* **460**(2046): 1597–1611.

Wu Z, Huang NE. 2005a. Ensemble empirical mode decomposition: a noise-assisted data analysis method. Centre for Ocean-Land-Atmospheric Studies Technical Report No. 193, Center for Ocean-Land-Atmosphere Studies, Calverton, MD, 1–51. ftp://grads.iges.org/pub/ctr/ctr 193.pdf (accessed 28 April 2014).

Wu Z, Huang NE. 2005b. Statistical significance test of intrinsic mode functions. In *Hilbert-Huang Transform and Its Applications*, Huang NE, Shen SP (eds). World Scientific: Hackensack, NJ, 125–148.

Wu Z, Huang NE, Long SR, Peng CK. 2007. On the trend, detrending and variability of nonlinear and non-stationary time series. *Proc. Natl. Acad. Sci. USA* **104**: 14889–14894.

Wu Z, Huang NE, Wallace JM, Smoliak BV, Chen XY. 2011. On the time-varying trend in the global mean surface temperature. *Clim. Dyn.* **37**: 759–773.

Zhang Y, Wallace JM, Battisti DS. 1997. ENSO-like inter-decadal variability. *J. Clim.* **10**: 1004–1020.

Zhen-Shan L, Xian S. 2007. Multi-scale analysis of global temperature changes and trend of a drop in temperature in the next 20 years. *Meteorol. Atmos. Phys.* **95**(1–2): 115–121.

